Ionics (2019) 25:2275–2283
https://doi.org/10.1007/s11581-018-2630-3

ORIGINAL PAPER

Electrochemical performance of CH_3COONa aqueous electrolytes

Siyun Huang[1] · Jianqiang Zhang[1] · Deyi Zhang[1] · Huixia Feng[1] · Heming Luo[1]

Received: 7 December 2017 / Revised: 10 June 2018 / Accepted: 11 June 2018 / Published online: 31 July 2018

Abstract

Supercapacitors are a promising high-power energy storage device due to highly reversible charge-storage process and long cyclic stability. However, the major limitation of supercapacitors lies in their energy density. Here, a high voltage carbon-based supercapacitor is built by using 2 M CH_3COONa aqueous solution as electrolyte. In three-electrode system, this paper uses the potentiostatic polarization curves to study the 1.8 V high operating voltage window with the nitrogen-self-doped mesoporous carbon materials (FBNC-700) as electrode materials. In two-electrode system, the FBNC-700 displayed a specific capacitance of 111 F g^{-1} at a current density of 0.5 A g^{-1} in 2 M CH_3COONa aqueous electrolyte. The 2 M CH_3COONa aqueous electrolytes which can improve the energy density to 3.8 times than the 1 M H_2SO_4 aqueous electrolyte exhibits an excellent performance. Also, following 5000 cycles at a current density of 1 A g^{-1}, the FBNC-700 had good stability with 74.2% capacitance retention. As an aqueous electrolyte, 2 M CH_3COONa which has the 1.8 V high operating voltage window can improve the energy density in carbon-based supercapactor.

Keywords Potentiostatic polarization curves · CH_3COONa · Aqueous electrolytes · Supercapacitor

Introduction

With higher requirements for carbon-based supercapacitor, the aqueous electrolyte and electrode material play an increasingly important role in improving the properties on supercapacitor, such as the energy density [1–3]. Recently, improving the energy density is not limited to the way that we optimize carbon materials properties to improve the energy density. To select a suitable aqueous electrolytes to improve the energy density is an important means. The energy density is proportional to the square of the operating voltage window in supercapacitor. It should be noted that enlarging the operating voltage window is remarkable to improve the energy density [4].

The aqueous electrolytes [5], when applied to supercapacitor, present several advantages over the organic ones [6]. The systems are cheaper, environment friendly, and easy to construct [7–9]. Moreover, with activated carbons (AC) enriched with heteroatoms (N [10], B [11], P [12], and S [13]), the capacitance can be enhanced through pseudocapacitive redox reactions between the surface functionalities and the aqueous electrolyte [14]. Compared with the organic ones, the aqueous electrolyte has lower operating voltage window which does not benefit improving the energy density. The salt solution, such as $LiNO_3$ [15] and K_2SO_4 [16], substitutes traditional aqueous electrolytes such as KOH and H_2SO_4 [17]. The 2 M $LiNO_3$ with 1.6 V operating voltage window [16] and the 2 M K_2SO_4 with 1.7 V operating voltage window plays an important role in improving the energy density. Studies show that the salt solution has great potential to substitute traditional aqueous electrolytes and improve the properties of carbon-based supercapacitor [15]. The salt solution will become a new aqueous electrolyte with high operating voltage window.

To enlarge the voltage window gradually, we find out the operating voltage window of new aqueous electrolytes. If the new aqueous electrolytes has larger operating voltage window, we would have a mammoth workload. It is a tedious way to study the operating voltage window of aqueous electrolytes [15, 16]. As a commonly electrochemical test, the potentiostatic polarization curves can test the stability of aqueous electrolytes [18]. When the electrode has polarity, the potentiostatic polarization curves have to deviate obviously and the surface of electrodes produces air bubbles. Through the cathodic polarization curve tests and the cathode polarization curve tests, we find out the negative potential of the water electrochemical decomposition and the anodic one. It is the

✉ Heming Luo
luohm666@163.com

[1] School of Petrochemical Engineering, Lanzhou University of Technology, Lanzhou, China

operating voltage window of aqueous electrolytes between the negative potential of the water electrochemical decomposition and the anodic one. The way the potentiostatic polarization curves test is more simple and accurate.

As a type of organic salt which is used in industry, CH_3COONa is used to printing industry [19], medical science [20], and so on [21]. It has excellent solubility and high degree of ionization. The CH_3COONa dissolves easily in water and its aqueous solution alkalescence [22].

This paper inspects the properties of CH_3COONa aqueous electrolytes, whereas the custom-made FBNC-700 is utilized as the electrode material [23]. As an organic salt aqueous, CH_3COONa aqueous which can be used as electrolytes has higher voltage window and lower cost. Moreover, the CH_3COONa aqueous as electrolytes increases electrolytes species. In three-electrode system, this paper uses the potentiostatic polarization curves to study the operating voltage window of CH_3COONa aqueous electrolytes. In the two-electrode system, the performance of FBNC-700-based supercapacitor at 1.8 V was evaluated using 2 M CH_3COONa aqueous electrolytes.

Experiments

Physical parameters of FBNC-700

The FBNC-700 was prepared through carbonization process of FAC-brown as reported previously (Fig. 1) [23].

The physical property parameter of theFBNC-700 is presented in Table 1. The pore-structure fractal characteristics on the nitrogen-self-doped mesoporous carbons are presented in Fig. 2 [24].

CH_3COONa aqueous electrolytes characteristics

The CH_3COONa aqueous can be made by CH_3COONa (AR, Tianjin Dingshengxin Chemical Industry) dissolved in the deionized water. The conductivity of aqueous electrolytes was investigated by electric conductivity analyzers (DDSJ-308F) in 25 °C. The pH of aqueous electrolytes was investigated by a pH tester ("SHANGHAI REX CO-PERFECT INSTRUMENT CO, LTD; pHS-3E).

Table 1 The physical property parameter of FBNC-700

Physical property parameter	Property
S_{BET} ($m^2\ g^{-1}$)	1021
$V_{totalpore}$ ($cm^3\ g^{-1}$)	1.38
Pore diameter (nm)	5.39
C/O/N (%)	87.45/10.53/2.02

CH_3COONa aqueous electrolytes electrochemical measurement

In order for the working electrode to be prepared, the FBNC-700 were ground with polytetrafluoroethylene (5 wt%) and consequently pressed onto a steel mesh (1 cm × 1 cm) functioning as a current collector. The carbons were subsequently dried in a vacuum at 80 °C for 12 h, whereas the working electrode was subsequently pressed at 15 MPa for 1–2 min. A conductive agent (such as acetylene black) was not required for the working electrode preparation.

The potentiostatic polarization curve ($J=f(E)$, E as electrode potential, J as current density) measurements including the cathodic polarization curve tests and the anodic polarization curve tests were performed under ambient conditions in aqueous electrolytes with the FBNC-700 as the working electrode, a platinum slice (1.5 cm^2) as the counter electrode, and a saturated calomel electrode as the reference electrode in the three-electrode system. The electrochemical measurements including the cyclic voltammetry (CV), the galvanostatic charge/discharge (GCD), and the electrochemical impedance spectroscopy (EIS) were performed under ambient conditions in aqueous electrolytes with the FBNC-700 as the working electrode and the counter electrode in the two-electrode system.

Furthermore, the anodic polarization curve tests were performed at the scan rates of 5 mV s^{-1} over a potential window of − 5 to 2 V. The cathodic polarization curve tests were performed at the scan rates of 5 mV s^{-1} over a potential window of − 2 to 0 V.

The GCD tests were performed at charge/discharge currents of 0.5~6 A g^{-1} over a potential window of − 1.1 to 0.7 V. The specific capacitance C (F g^{-1}) of the samples was calculated as presented in Eq. 1:

$$C = \frac{I*\Delta t}{m*\Delta V}\cdot 4\cdot \frac{1}{2} \tag{1}$$

where I is the constant discharging current (A), Δt is the discharge duration (s) period for the potential change ΔV (V), and m (g) is the mass of the nitrogen-self-doped mesoporous carbons in the electrode.

The CV was performed at the scan rates of 5–80 mV s^{-1}over the potential window of − 1.1 to 0.7 V. The specific capacitance C (F g^{-1}) was also calculated from the CV curves according to Eq. 2:

$$C = \frac{\int I\ dV}{2*vm\Delta V}\cdot 4\cdot \frac{1}{2} \tag{2}$$

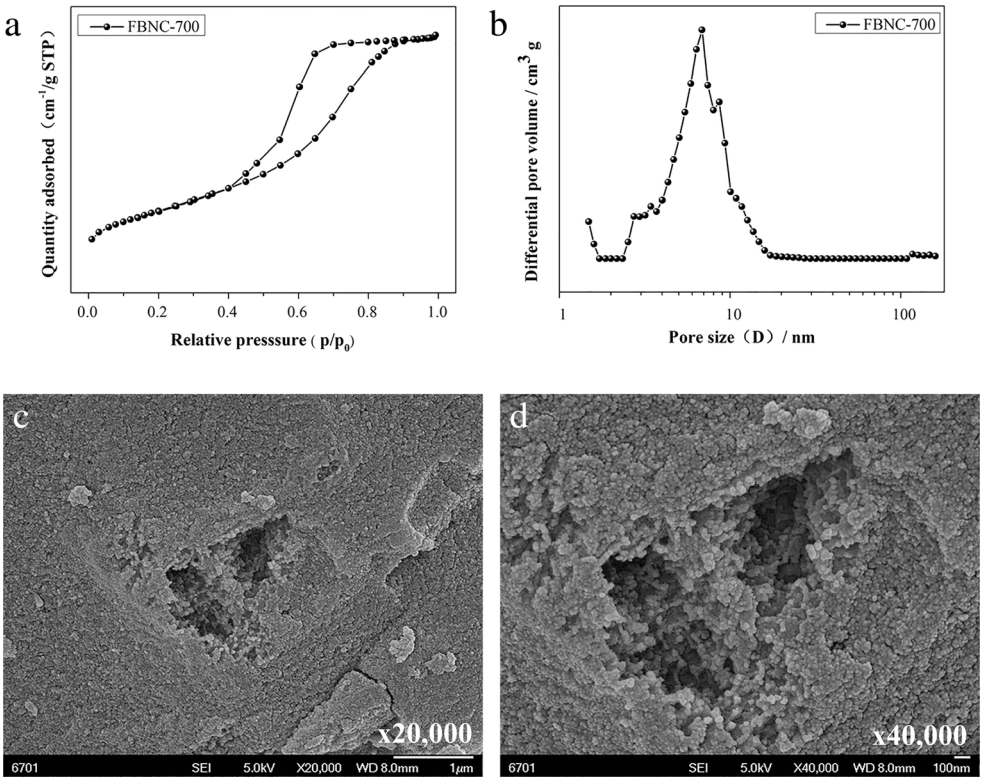

Fig. 1 **a** The nitrogen adsorption isotherms of FBNC-700. **b** The pore size distribution of FBNC-700. **c**, **d** The SEM of FBNC-700

where I is the current as a function of voltage and ν is the scan rate (V s^{-1}).

The EIS measurements were performed at the open-circuit potential with an AC amplitude of 5 mV within the frequency range of 10^{-2}~100 Hz.

The energy density is calculated by Eq. 3:

$$E = \frac{1}{2} \cdot CU^2 \tag{3}$$

where U is the potential window (V).

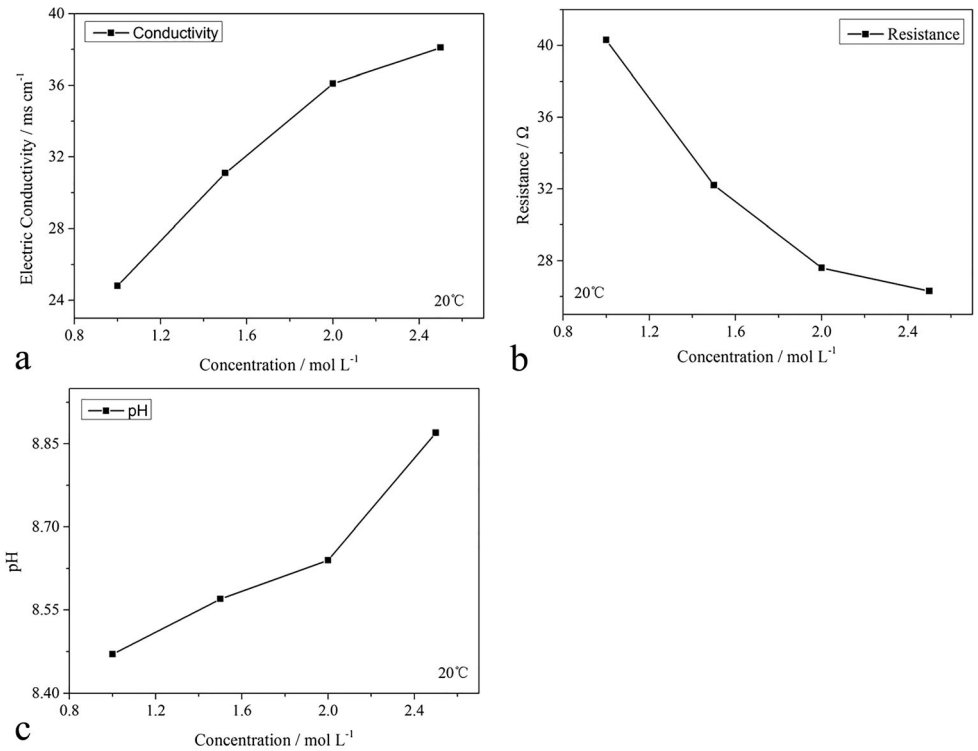

Fig. 2 The physical and chemical properties ofCH_3COONa aqueous solutions. **a** pH. **b** Conductivity. **c** Resistance

Results and discussion

CH_3COONa aqueous electrolytes physical and chemical properties

Figure 2 presents the physical and chemical properties of the CH_3CH_2COONa aqueous solutions. Due to fact that the CH_3COONa was a product of a strong base with a weak acid salt, it should sustain hydrolysis. Also, the hydrolysis formation is presented in Eq. 4:

$$CH_3COONa + H_2O \leftrightarrow CH_3COOH + Na^+ + OH^- \quad (4)$$

$$CH_3COONa \leftrightarrow CH_3COO^- + Na^+ \quad (5)$$

When the concentration was 2 M, the pH_{2M} was 8.64 ($\Delta pH = 0.03$) at 25 °C, in Fig. 2a. The CH_3COONa aqueous solution was a weak alkaline substance that produced the anodic passivation to increase in the anodic polarization curve tests. After 2 M CH_3COONa, the trend of increasing becomes more quickly with concentrations increasing. The pH signified the relationship between hydrolysis of CH_3COONa and the ionization (Eq. 5). As shown in Fig. 2a, the ionization of 2.5 MCH_3COONa becomes weak. The conductibility and resistance of CH3COONa aqueous solutions have similar trends, as shown in Fig. 2b, c. The trend becomes more slowly with concentrations increasing because of the relationship between hydrolysis of CH_3COONa and the ionization. When the concentration was 2 M, the conductivity of is 36.1 mS cm^{-1} and the resistance is 27.0 Ω.

The cathodic polarization curve tests

In Fig. 3c, when the current passed through the cathodic electrode, the electrode potential moved to the negative electrode potential, and the cathodic potential E_K was of a higher negative value than the equilibrium potential of cathodic electrode $E_{K,e}$,$\Delta E < 0$ (Eq. 6).

$$\Delta E = E_K - E_{K,e} \quad (6)$$

The chemical equilibrium of the cathodic electrode is provided in Eq. 7.

$$2H_2O + 2e^- \rightarrow H_2\uparrow + 2OH^- \quad (7)$$

As the cathodic potential moved to the negative electrode potential at the scan rates of 5 mV s^{-1}, the current density(J) sustained a gradual deviation from 0 in the electrochemical tests. The water electrochemical decomposition did not occur on the electrode surface when $E \geq -1.1$ V in Fig. 3c. At this point, the electrolyte was stabilized at $\Delta \leq 0.01$ A. The water electrochemical decomposition occurred when $\Delta > 0.01$ A. Bubbles could be observed to increase in size on the electrode surface, as Eq. 7. At this point, the electrolyte was not stabilized at $E < -1.1$ V. It was demonstrated that the −1.1 V was the negative potential of the water electrochemical decomposition.

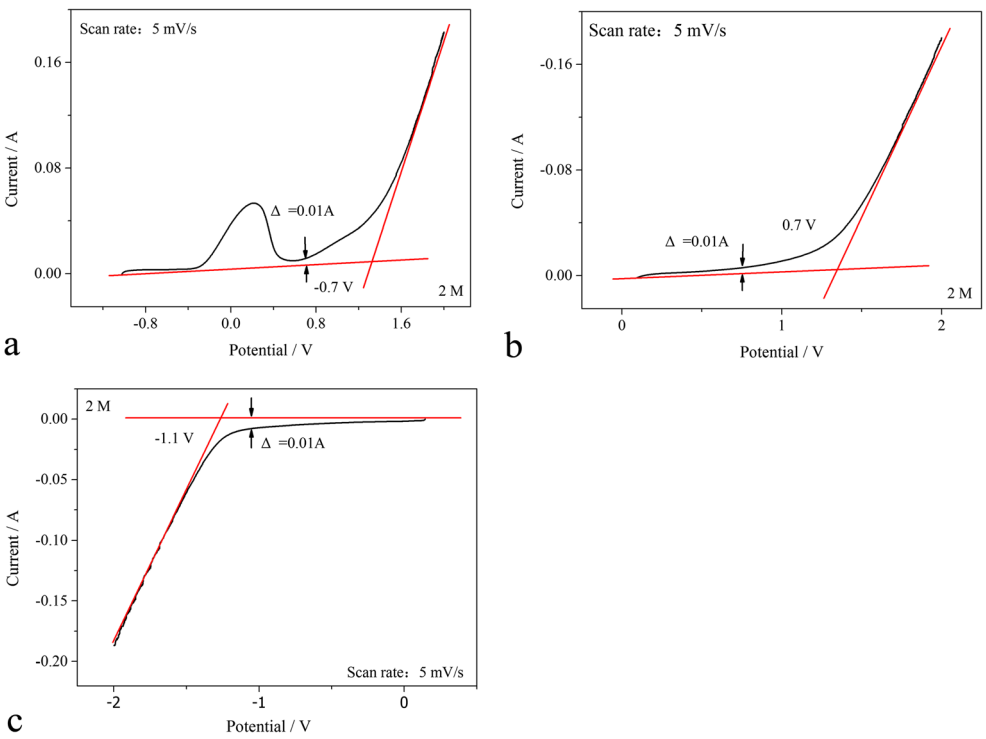

Fig. 3 The polarization curve tests of the 2 M CH_3COONa aqueous electrolytes with three electrodes system. **a** The cathodic polarization curve tests. **b** The cathode polarization curve tests. **c** The anodic polarization curve tests for the second time

The anodic polarization curve tests in the first time

When the current passed through the anodic electrode, the electrode potential moved to the positive electrode potential, whereas the anodic potential E_A was significantly positive in value than the equilibrium potential of the anodic electrode $E_{A,e}$,$\Delta E > 0$ (Eq. 8) [25, 26].

$$\Delta E = E_A - E_{A,e} \tag{8}$$

The chemical equilibria of the anodic electrode, is presented in Eq. 9.

$$4OH^- \rightarrow O_2\uparrow + 2H_2O + 4e^- \tag{9}$$

In Fig. 3a, as the anodic potential moved to the positive electrode potential at the scan rate of 5 mV s^{-1}, the current density (J) has a gradual deviation from − 0.8 V in the electrochemical tests. It was noted that a significant peak at approximately − 0.25 V existed. This phenomenon was referred to as "anodic passivation" [27]. The anodic passivation is electronic behavior which protects the anodic.

As the anodic potential moved to the positive electrode potential at the scan rates of 5 mV s^{-1}, the water electrochemical decomposition did not occur on the electrode surface when $E \leq$ 0.7 V in Fig. 3a. At this point, the electrolyte was stabilized at $\Delta \leq 0.01$ A. The water electrochemical decomposition occurred when $\Delta > 0.01$ A. Bubbles could be observed to increase in size on the electrode surface, as Eq. 9. At this point, the electrolyte was not stabilized at $E > 0.7$ V. It was demonstrated that the − 0.7 V was the anodic potential of the water electrochemical decomposition.

Anodic polarization curve tests in the second scan

The anodic polarization curve tests for the CH_3COONa aqueous electrolyte in the second scan are presented in Fig. 3b. Apparently, the anodic passivation was weakened in these anodic polarization curve tests. The overpotential scanning in the anodic polarization curve tests disturbed the surface functional groups of activated carbon. Subsequently to the anodic polarization curve tests, the surface functional groups of the activated carbon were affected by the overpotential. The electrode surface became significantly hydrophilic compared to the corresponding previous state. This phenomenon constituted the effects between the electrode surface and the

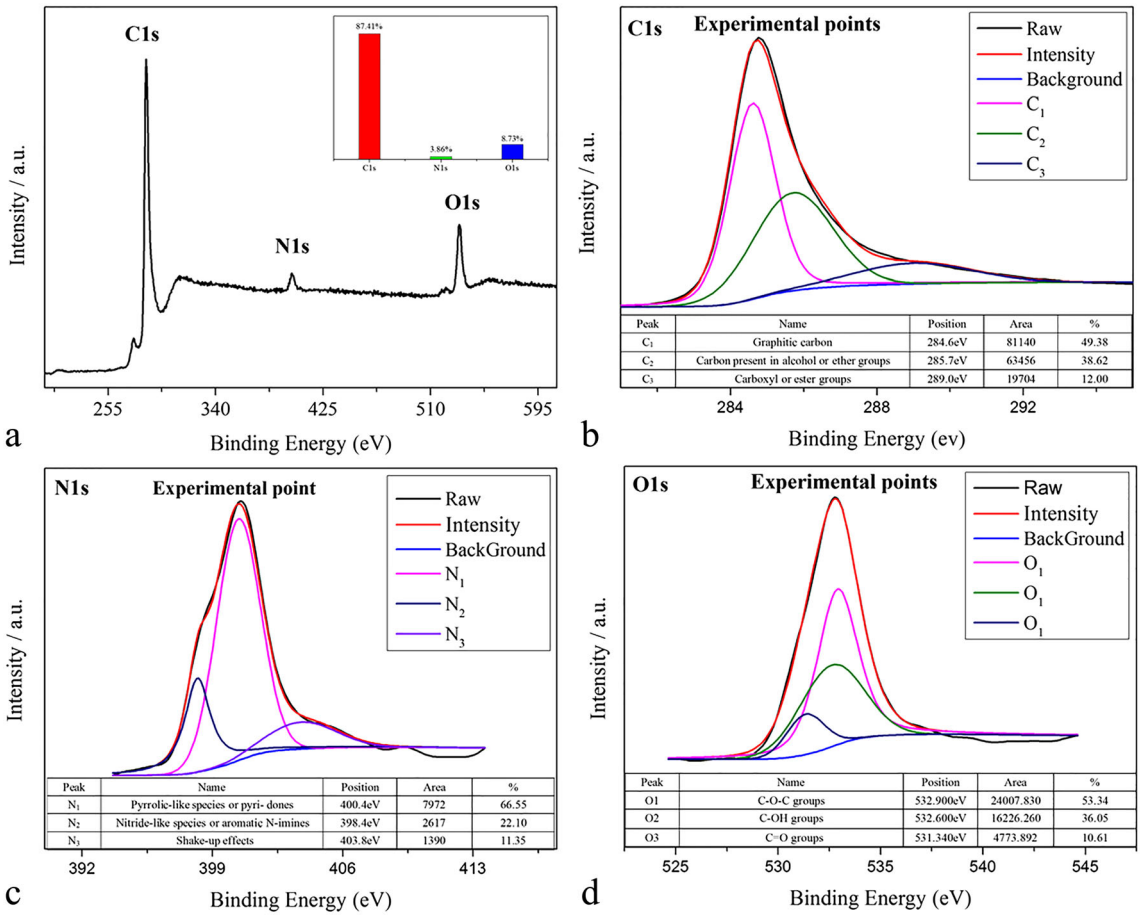

Fig. 4 **a** XPS survey, **b** C1s, **c** N1s, and **d** O1s XPS spectra of FBNC-700 before the anodic polarization curve tests

electrolyte to be lower than before. The electrolyte was easier to diffuse. Therefore, the anodic passivation was weakened in the anodic polarization curve tests second execution. The surface functional groups change would not be restored. This conclusion had a high degree of consistency with the XPS results following the overpotential scanning tests.

FBNC-700 characterization by XPS techniques following overpotential scanning tests

In the Figs. 4a and 5a, the content of C, O, and N in the FBNC-700 had a significant change following the overpotential scanning. Due to the overpotential scan, the carbon of the FBNC-700 was partially lost. Also, the contents of O and N in the FBNC-700 became quite diverse. Also, a certain functional group changing occurred in the C, O, and N [28].

Regarding the carbon, as shown in Figs. 4b and 5b, the carbon could not only retain the corresponding original form, such as the graphite carbon, carbon present in alcohol, or ether groups and or ester groups, but also can be presenting other form such as carboxyl after being overpotential scanning [29]. A high amount of carbonyl groups improved the hydrophilicity. The effects between the electrode surface and the electrolyte became lower than before. The electrolyte was easier to wet.

Regarding the nitrogen, as shown in Figs. 4c and 5c, the nitrogen could not only retain the corresponding original form, such as pyrrolic-like species or pyridones, pyridine-N-oxide species, the nitride-like species, or aromatic N-imines [30]. Following the overpotential scanning, it possibly exists in other forms such as the pyrrolic-like species or pyrrolic. The pyrrolic structures and pyrrolic-like species could improve the conductibility and reduce the FBNC-700 internal resistance. The former could be beneficiary to the ion transfer.

Regarding the oxygen, as shown in Figs. 4d and 5d, the C-O-C content decreased and the content of C=O increased [31]. The quantitative change in the form of O demonstrated that the surface oxygen functional groups were shattered and the carbon surface was oxidated subsequently to the overpotential scanning. Also, the carbon of the FBNC-700 was partially lost due to the latter phenomenon. Additionally important, the higher amount of C=O which could be shown in Fig. 5d could improve the pseudocapacitance by the redox peaks at 0.4 V. The higher amount of C-OH makes the FBNC-700 easier to wet by 2 M CH_3COONa aqueous electrolyte.

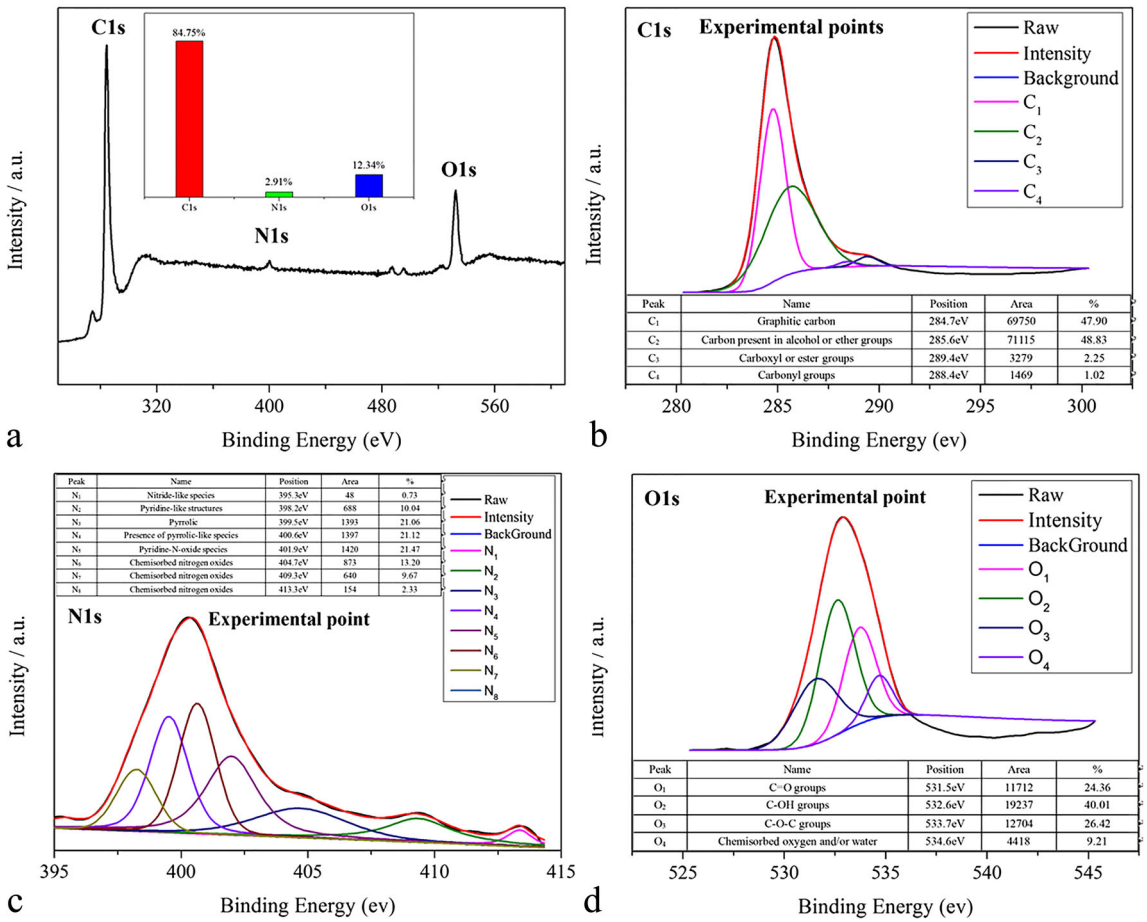

Peak	Name	Position	Area	%
C_1	Graphitic carbon	284.7eV	69750	47.90
C_2	Carbon present in alcohol or ether groups	285.6eV	71115	48.83
C_3	Carboxyl or ester groups	289.4eV	3279	2.25
C_4	Carbonyl groups	288.4eV	1469	1.02

Peak	Name	Position	Area	%
N_1	Nitride-like species	395.3eV	48	0.73
N_2	Pyridine-like structures	398.2eV	688	10.04
N_3	Pyrrolic	399.5eV	1393	21.06
N_4	Presence of pyrrolic-like species	400.6eV	1397	21.12
N_5	Pyridine-N-oxide species	401.9eV	1420	21.47
N_6	Chemisorbed nitrogen oxides	404.7eV	873	13.20
N_7	Chemisorbed nitrogen oxides	409.3eV	640	9.67
N_8	Chemisorbed nitrogen oxides	413.3eV	154	2.33

Peak	Name	Position	Area	%
O_1	C=O groups	531.5eV	11712	24.36
O_2	C-OH groups	532.6eV	19237	40.01
O_3	C-O-C groups	533.7eV	12704	26.42
O_4	Chemisorbed oxygen and/or water	534.6eV	4418	9.21

Fig. 5 **a** XPS survey, **b** C1s, **c** N1s, and **d** O1s XPS spectra of FBNC-700 after the anodic polarization curve tests

The CH_3COONa aqueous electrolyte electrochemical performance test in two electrode system

The application performance of electrolytes could be utilized for the GCD evaluation. In Fig. 6a, as expected, the isosceles triangle on the GCD of the FBNC-700, which deviated from linearity, demonstrated the corresponding excellent charge-discharge reversibility. It was observed that the voltage window range between 0.7 and − 1.1 V was feasible and the electrical double layer could be formed in the CH_3COONa aqueous electrolytes. The polarization curve tests demonstrated that the voltage window of CH_3COONa ranged from 0.7 to − 1.1 V which is practicable. Under various current densities, the FBNC-700 sustained the GCD in Fig. 6b. It was observed that the 2 M was the optimized concentration of the CH_3COONa aqueous. In Fig. 6c, the CV sustained stability transformation when the voltage window was produced. The FBNC-700 displayed the stability electrochemical behavior in the CH_3COONa aqueous electrolytes. It was observed that the voltage window range between 0.7 and − 1.1 V was feasible.

Table 2 The voltage window of different aqueous electrolytes

Aqueous electrolytes	Operating voltage range	Voltage window
KOH	− 1~0 V	1 V
H_2SO_4	0~1 V	1 V
Na_2SO_4	− 0.6~0.7 V	1.1 V
Li_2SO_4	− 0.6~0.7 V	1.1 V
K_2SO_4	− 0.6~0.7 V	1.1 V
CH_3COONa	− 0.8~1.1 V	1.3 V

In Table 2 and Fig. 6b, the 2 M CH_3COONa aqueous electrolytes demonstrated improved capacity and rate discharge performance. Good specific capacitance of 111 F g^{-1} at 0.5 A g^{-1}

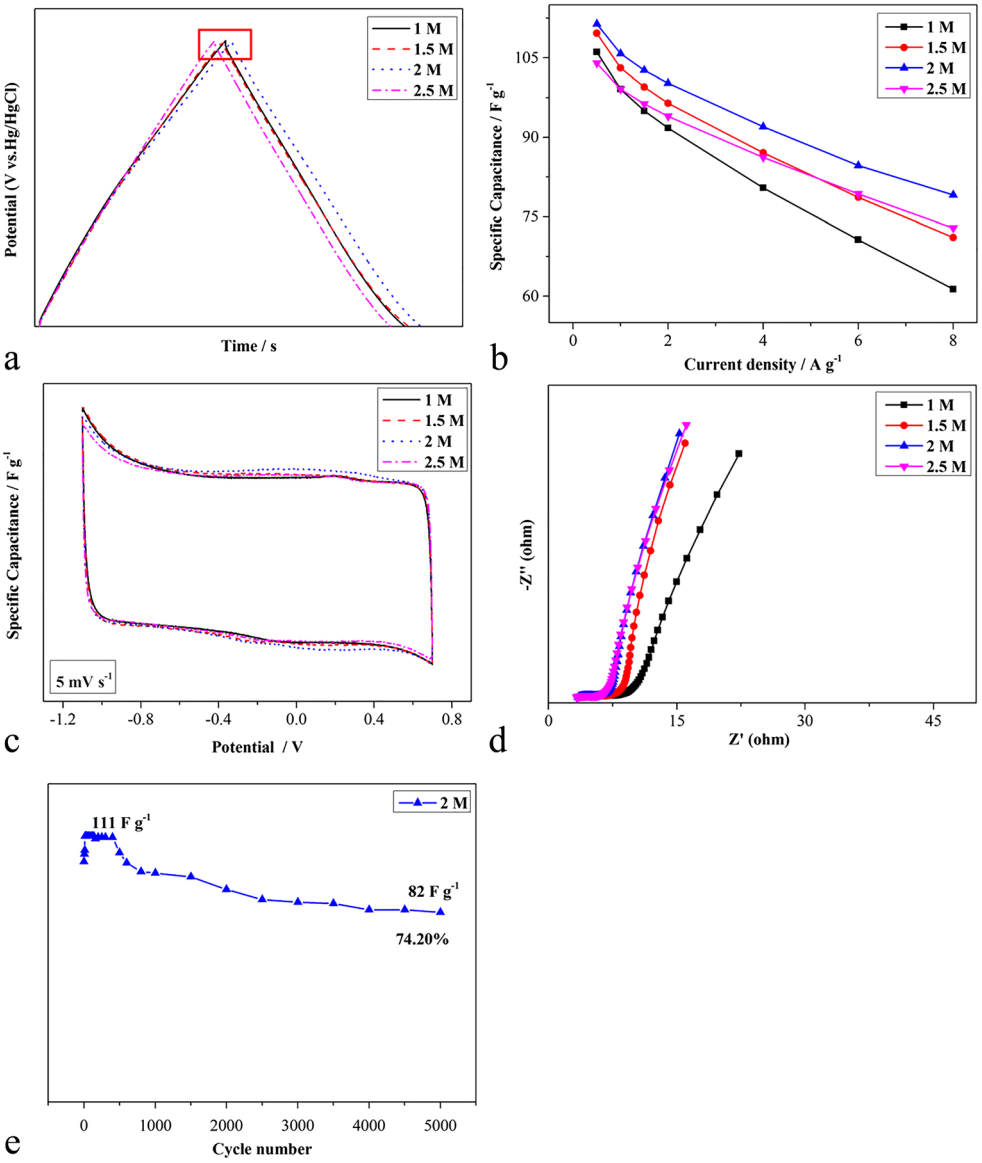

Fig. 6 The electrochemical performance of CH_3COONa with two electrodes system. **a** The GCD. **b** The capacitance performance at different current density. **c** The CVs. **d** The impedance test. **e** The cycle life test of 2 M CH_3COONa at 1 A g^{-1}

was achieved using FBNC-700. The higher specific capacitance came from the 2 M CH_3COONa aqueous because of the higher voltage window of 1.8 V. The higher voltage window can expand the range of the charge-discharge. Moreover, the redox reaction is promoted by higher voltage because of the higher voltage window. The higher specific capacitance can be made. Following 5000 charge-discharge cycles, a high electrochemical stability and improved capacitance retention rate was observed (74.2%), as shown in Fig. 6e.

Figure 6d presents the Nyquist diagram of the FBNC-700 in the CH_3COONa aqueous electrolytes. At high frequency, the curves of 1, 1.5, 2, and 2.5 M were approximately perpendicular to the real axis, indicating that the ions of CH_3COONa aqueous could facilitate a quick diffusion in porous materials. The 1 M curve deviated highly under a high frequency, which demonstrated the strong resistance against the electrolyte ion diffusion, due to a low concentration of the ions. Apparently, the 2 M CH_3COONa aqueous electrolyte reached an excellent capacitive performance in the high-frequency region with the increase of frequency. This phenomenon could be explained in Fig. 1. The relationship between hydrolysis of CH_3COONa and the ionization plays important role in ions transmission.

2 M CH_3COONa aqueous electrolye electrochemical performance compares with 1 M H_2SO_4 in the two-electrode system

In Fig. 7a, the higher specific capacitance came from the 2 M CH_3COONa aqueous because of the higher voltage window of 1.8 V. As shown in Fig. 7b, as a type of aqueous electrolyte, 2 M CH_3COONa which has the 1.8 V high operating voltage window has bigger specific capacitance than 1 M H_2SO_4 at 5 A g^{-1}. By Eq. 3, the high operating voltage window can improve the energy density. At 5 A g^{-1}, 2 M CH_3COONa can improve 3.8 times for energy density in Fig. 7c. In Fig. 7d, 2 M CH_3COONa has bigger horizontal intercept than 1 M H_2SO_4 aqueous electrolytes, for the bigger ionic radius. So, the CH_3COO^- could not form the electrical double layer quickly. In high frequency, the ratio of 2 M CH_3COONa aqueous electrolyte is higher than 1 M H_2SO_4. It is because that 2 M CH_3COONa aqueous electrolyte has more ions.

In Table 2, the CH_3COONa has higher voltage window than other aqueous electrolytes. In Eq. 3, the higher operating voltage window can remarkably improve the energy density which can be shown in Fig. 7c.

Conclusions

This paper was devoted the potentiostatic polarization curves to study the voltage window of aqueous electrolytes which is a simple way. In three-electrode system, the 2 M CH_3COONa aqueous demonstrated 1.8 V high operating voltage window and an excellent electrochemical performance. In the 2 M CH_3COONa aqueous electrolyte, the FBNC-700 displayed a 111 F g^{-1} specific capacitance at the current density of 0.5 A g^{-1} in the two-electrode tests. The bigger specific capacitance and higher operating voltage window can improve

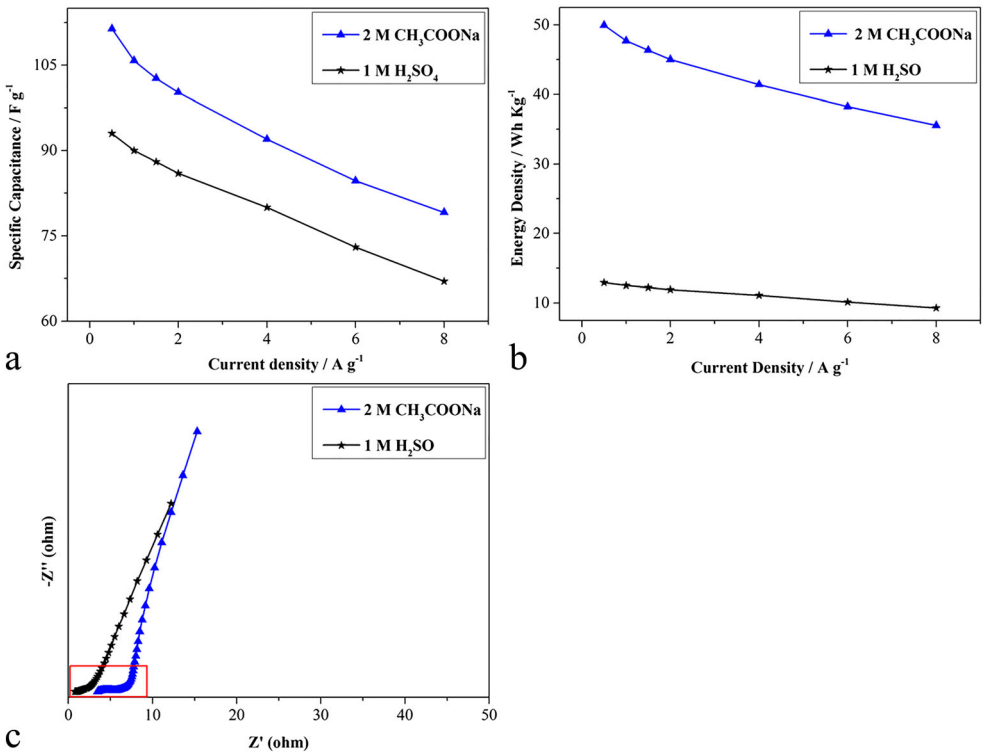

Fig 7 The comparison of electrochemical performance between 2 M CH_3COONa and 1 M H_2SO_4 in two electrodes. **a** The CVs. **b** The comparison of GCD at different current densities. **c** The comparison of energy density. **d** The comparison of impedance test

3.8 times for energy density. Also, following 5000 cycles at a current density of 1 A g^{-1}, the FBNC-700 displayed good stability with 74.2% capacitance retention.

Funding information This work is partially supported by the fund of National Nature Science Foundation of China (No. 201664009) and the National Natural Science Foundation of China (No. 51462020).

References

1. Liu C, Yu Z, Neff D, Zhamu A, Jang BZ (2010) Graphene-based supercapacitor with an ultrahigh energy density. Nano Lett 10: 4863–4868
2. Zhang LL, Zhao XS (2009) Carbon-based materials as supercapacitor electrodes. Chem Soc Rev 38:2520–2531
3. Shiue LR, Cheng CS, Chang JH, Li LP, Lo WT, Huang KF. Supercapacitor with high energy density. J Appl Phys 122(21): 214902
4. Novikau U (2016) Improving Supercapacitor energy density via Nanocarbon electrode functionalization and increasing electrolyte electrochemical window. Materials Research Society Advances 1: 1377–1382
5. Ghosh S, Mathews T, Gupta B, Das A, Gopalakrishna N, Kamruddin M (2017) Supercapacitive vertical graphene nanosheets in aqueous electrolytes. Nano-Structures and Nano-Objects 10:42–50
6. Jian-Ling LI, Liang J, Jing-Ming XU, Mao ZQ (2001) Progress on the studies on organic electrolytes for electric double-layer capacitor. Chinese Journal of Power Sources 3:229–234
7. Hulicova D, Yamashita J, Soneda Y, Hiroaki Hatori A, Kodama M (2005) Supercapacitors prepared from melamine-based carbon. Chem Mater 17:1241–1247
8. Raymundo-Piñero E, Leroux F, Béguin F (2010) A high-performance carbon for Supercapacitors obtained by carbonization of a seaweed biopolymer. Adv Mater 18:1877–1882
9. Hulicovajurcakova D, Puziy AM, Poddubnaya OI, Suárezgarcía F, Tascón JM, Lu GQ (2009) Highly stable performance of supercapacitors from phosphorus-enriched carbons. J Am Chem Soc 131:5026–5027
10. Yang G, Chen H, Qin H, Feng Y (2014) Amination of activated carbon for enhancing phenol adsorption: effect of nitrogen-containing functional groups. Appl Surf Sci 293:299–305
11. Guo H, Gao Q (2009) Boron and nitrogen co-doped porous carbon and its enhanced properties as supercapacitor. J Power Sources 186: 551–556
12. Puzii AM, Stavitskaya SS, Poddubnaya OI, Vikarchuk VM, Tsyba NN (2012) Structural and adsorption properties of active carbon from coconut shells modified with phosphorus heteroatoms. Theor Exp Chem 48:272–277
13. Liu S, Tong M, Liu G, Zhang X, Wang Z, Wang G, Cai W, Zhang H, Zhao H (2016) S, N-containing co-MOFs derived Co_9S_8@S,N-doped carbon materials as efficient oxygen Electrocatalysts and Supercapacitor electrode materials. Inorg Chem Front 4:491–498
14. Augustyn V, Simon P, Dunn B (2014) Pseudocapacitive oxide materials for high-rate electrochemical energy storage. Energy Environ Sci 7:1597–1614
15. Luo HM, Yang YF, Mu B, Chen YZ, Zhang JQ, Zhao X (2016) Facile synthesis of microporous carbon for supercapacitors with a LiNO 3 electrolyte. Carbon 100:214–222
16. Qu QT, Wang B, Yang LC, Shi Y, Tian S, Wu YP (2008) Study on electrochemical performance of activated carbon in aqueous Li_2SO_4, Na_2SO_4 and K_2SO_4 electrolytes. Electrochem Commun 10:1652–1655
17. Hanappi MFYM, Deraman M, Suleman M, Nor NSM, Sazali NES, Hamdan E, Tajuddin NSM, Basri NH, Jasni MRM, Othman MAR (2017) Influence of aqueous KOH and H_2SO_4 electrolytes ionic parameters on the performance of carbon-based supercapacitor electrodes. Funct Mater Lett 10:49
18. Kitamura Y, Suzuki C, Okano K (2009) Interrelation between cell voltage-current curves and Potentiostatic polarization curves. Corros Eng 12:278–282
19. Pelster G, Schidlo W (1992) Single-step printing of cellulose fibers with triphen-dioxazine reactive dyes and with sodium acetate or sodium trichloro-acetate as alkali. US, US5085668
20. Li-Na AN, Xue J, Shu-Ping S (2016) Experimental study on denitrification effect of SBBR with sodium acetate as external carbon source. Contemporary Chemical Industry 45:22–24
21. Mao J, Dong X, Hou P (2017) Preparation research of novel composite phase change materials based on sodium acetate trihydrate. Appl Therm Eng 118:817–825
22. Merrill MD, Montalvo E, Campbell PG, Wang YM, Stadermann M, Baumann TF, Biener J, Worsley MA (2014) Optimizing supercapacitor electrode density: achieving the energy of organic electrolytes with the power of aqueous electrolytes. RSC Adv 4: 421–435
23. Luo H, Chen YZ, Wang B, Zhang J, Zhao X, Mu B (2017) Nitrogen-self-doped mesoporous carbons synthesized by the direct carbonization of ferric ammonium citrate for high-performance supercapacitors. J Solid State Electrochem 21:515–524
24. East M (2016) Physisorption of gases, with special reference to the evaluation of surface area and pore size distribution. Chem Int 38: 25–25
25. Ke XU, Wang S (2000) The testing analysis of the electric polarization curves of the Pt-C compound electrodes made by different techniques. Journal of Xian Highway University 4:126–129
26. Devereux OF (1979) Polarization curve-fitting by computer modelling. United States. https://doi.org/10.5006/0010-9312-35.3.125
27. Shutt WJ (1935) Anodic passivation. Trans Faraday Soc 31: 636–637
28. Lee YH, Chang KH, Hu CC (2013) Differentiate the pseudocapacitance and double-layer capacitance contributions for nitrogen-doped reduced graphene oxide in acidic and alkaline electrolytes. J Power Sources 227:300–308
29. Rivera-Utrilla J, Sánchez-Polo M, Gómez-Serrano V, Álvarez PM, Alvim-Ferraz MCM, Dias JM (2011) Activated carbon modifications to enhance its water treatment applications. An overview. J Hazard Mater 187:1–23
30. Biniak S, Szymański G, Siedlewski J, tkowski AŚjm (1997) The characterization of activated carbons with oxygen and nitrogen surface groups. Carbon 35:1799–1810
31. Jansen RJJ, Bekkum HV (1995) XPS of nitrogen-containing functional groups on activated carbon. Carbon 33:1021–1027